Published in final edited form as:
*Magn Reson Med*. 2009 February ; 61(2): 467–472. doi:10.1002/mrm.21819.

# Quantitative assessment of DTI-based muscle fiber tracking and optimal tracking parameters

**Anneriet M. Heemskerk**[1,2], **Tuhin K. Sinha**[1,2], **Kevin J. Wilson**[1], **Zhaohua Ding**[1,2,3,4,6], and **Bruce M. Damon**[1,2,4,5,6]

[1]Institute of Imaging Science, Vanderbilt University, Nashville, TN, United States

[2]Department of Radiology and Radiological Sciences, Vanderbilt University, Nashville, TN, United States

[3]Department of Electrical and Computer Engineering, Vanderbilt University, Nashville, TN, United States

[4]Department of Biomedical Engineering, Vanderbilt University, Nashville, TN, United States

[5]Department of Molecular Physiology and Biophysics, Vanderbilt University, Nashville, TN, United States

[6]Department of Program in Chemical and Physical Biology, Vanderbilt University, Nashville, TN, United States

## Abstract

Diffusion tensor imaging based fiber tracking in skeletal muscle has been used to reconstruct and quantify muscle architecture. In addition, the consistent pattern of muscle fiber geometry enables a quantitative assessment of the fiber tracking. This work describes a method to determine the accuracy of individual muscle fiber tracts based on the location at which the fibers terminate, the fiber path, and similarity to the neighboring fibers. In addition, the effect of different stop criteria settings on this quantitative assessment was investigated. Fiber tracking was performed on the tibialis anterior muscle of 9 healthy subjects. Complete fiber tracts covered 89.4 ± 9.6% and 75.0 ± 15.2% of the aponeurosis area in the superficial and deep compartments, respectively. Applications of the method include the exclusion of erroneous fiber tracking results, quantitative assessment of data set quality, and the assessment of fiber tracking stop criteria.

## Introduction

Diffusion tensor imaging (DTI)-based muscle fiber tracking enables reconstruction of muscle architecture (1–5). For elongated structures such as muscle fibers, the diffusion coefficient of water is greater along the fiber than perpendicular to it. By measuring the diffusion in at least six directions, a diffusion tensor can be calculated from which the main direction of diffusion can be extracted. This directional information can be combined with that of neighboring pixels to allow reconstruction of the fiber trajectory. This enables the estimation of muscle architectural parameters such as pennation angle, fiber length and physiological cross-sectional area (CSA) (1,2,4).

The arrangement of fibers within the muscle makes it an ideal target to study the accuracy of reconstructed fibers. Muscle fibers are aligned parallel to each other and do not diverge,

Address for correspondence: Anneriet M. Heemskerk, PhD, Vanderbilt University Institute of Imaging Science, 1161 21st Ave. S., AA 1105 MCN, Nashville, TN 37232-2310, Phone: 615 343-0465, Fax: 615 322-0734, E-mail: a.m.heemskerk@vanderbilt.edu.

cross or kiss, as white matter tracts do. In addition, the fibers within most muscles run from a point of origin to a point of insertion. For example, the bipennate tibialis anterior (TA) muscle fibers run from either the tibia or the superficial fascia of the anterior compartment to the central aponeurosis. This consistent alignment and the knowledge of start and end points of fibers enable a quantitative assessment of fiber tracking.

Besides the underlying muscle fiber paths, the reconstructed trajectories can also depend on intrinsic muscle properties (e.g. fat infiltration), image acquisition and artifacts (e.g. noise, partial volume artifacts, or eddy current effects) (6), and the fiber tracking algorithm and settings (e.g. deterministic versus probabilistic methods, or stop criteria parameters) (7). All these factors can contribute to early termination of the fiber tract or to the estimation of an incorrect path. So far no experimental studies have been reported showing a quantitative analysis of fiber tracking and the occurrence of incorrect fibers. Assessment of this type of quantitative analysis would add in the understanding of the influences of image acquisition parameters, stop settings, and tracking algorithm and provide a measure to compare tracts. Moreover, this assessment is needed when fiber reconstruction is used to calculate accurate architectural parameters.

In this work we propose a method to determine the accuracy of individual muscle fiber tracts based on the location at which the fibers terminate, the fiber path, the fiber length, and similarity to the neighboring fibers. In addition, we investigated the effect of different stop criteria settings on this assessment.

## Quantitative assessment of fiber tracking

The fiber tracking procedure we used is described by Lansdown et al. (4) and in short uses a mesh definition of the aponeurosis as the seed surface for fiber tracking, the formation of a mask to define the muscle boundaries and as stop criterion for fiber tracking, and the generation of up to 40,000 fiber tracts in the superficial and deep compartments of the muscle according to a streamlining algorithm. The quantitative assessment of fiber tracking consists of the following steps.

1. Determine the total number of propagated fiber tracts that have at least 2 neighboring fiber tracts (FT=100%).
2. Exclude fiber tracts that have less than six tracked steps (<9 mm; $FT_{Short}$).
3. Exclude fibers tracts that are tracked to the wrong side of the aponeurosis ($FT_{Crossed}$). To exclude these, two additional masks were formed based on the position of the superficial aspect of the aponeurosis or the deep aspect of the aponeurosis (see Figure 1). If a point along the fiber tract falls within the mask of the other compartment, the whole tract is excluded.
4. Exclude fiber tracts that differ by more than three steps (4.5 mm) in length from the median of their 24 neighboring tracts ($FT_{Length}$). A fixed length rather than the standard deviation is used to maintain similar criteria throughout the muscle and the use of the three step criterion accounts for variations due to discrete step size and partial volume effects.
5. Include all fiber tracts that terminate at or near the muscle border ($FT_{Complete}$). In general, we anticipate that completely propagated fiber tracts will extend fully from the aponeurosis to the muscle border, as defined in the anatomical images. However, the lower resolution of the DTI images than of the anatomical images will result in higher levels of partial volume artifact in the DTI images than in the anatomical images. When the fiber orientations of neighboring muscles differ from those of the TA, the FA will be reduced and the orientation of the principal

eigenvector will differ from elsewhere in the TA. The use of FA and curvature as stop criteria may thus cause fiber tracking to terminate near, but not at, the muscle border. Therefore, we consider that fiber tracts that have terminated at or within two voxels of the muscle border to have propagated completely (Figure 1).

6. Exclude the remaining fiber tracts, which we consider to have stopped prematurely for reasons such as high curvature between successive points or low FA ($FT_{Premature}$=100-$FT_{Short}$-$FT_{Crossed}$-$FT_{Length}$-$FT_{Complete}$).

## Methods

### Subjects

Nine healthy subjects (5 male) participated in this study. Their age was 29 ± 7 years (mean ± SD), with height 172 ± 12 cm and mass 69 ± 23 kg. The subjects lay supine with the right foot strapped into a custom-built exerciser at 15 degrees of plantar flexion. All procedures were approved by the Vanderbilt University Institutional Review Board, and written consent of the risk, benefits, and procedures was obtained from each subject prior to participation.

### MRI

Data were obtained with a Philips 3T scanner (Philips Medical Systems, Best, The Netherlands) using two double flexible surface coils covering the length of the TA muscle.

For anatomical reference a proton density (PD) weighted scan was obtained using field of view (FOV) = 196 × 196 $mm^2$, matrix size = 256 × 128 with 512 × 512 reconstruction, slice thickness = 6 mm, inter-slice gap = 0, 55 slices, repetition time (TR) = 4152 ms, echo time (TE) = 11 ms, number of excitation ($N_{EX}$) = 1.

DTI images were acquired in 5 continuous stacks of 11 slices each. The position of the bed was moved such that the center of each stack was located at the magnet isocenter and a sensitivity encoding (SENSE) reference scan was obtained for each stack. Scans were acquired using an EPI sequence with FOV = 192 × 192 $mm^2$, matrix size = 96 × 64 with 128 × 128 reconstruction, slice thickness = 6 mm, TR = 3300 ms, TE = 48 ms and SENSE factor = 1.2. The resulting voxel dimensions were 6 × 1.5 × 1.5 mm; we consider that this anisotropy had minimal effect on the fiber tracking results as the muscle fiber orientations in the laboratory frame of reference for the TA muscle do not vary over the muscle (4). Fat suppression was performed using inversion recovery with the fat-shift direction set so that residual fat signals were outside of the fiber tracking region. Diffusion weighted (DW) images were acquired with b = 500 s/$mm^2$ and in ten directions (8). The total scan time for all stacks was 15 minutes.

After the DTI a $T_2$ weighted ($T_2W$) scan was acquired for registration purposes with same geometric parameters as the PD scan and TR = 7557 ms, TE = 30 ms, $N_{EX}$ = 1, and inversion recovery based fat saturation.

### Image registration

Registration consisted of four steps: 1) within each stack, DW images to b=0; 2) DTI stacks to each other; 3) $T_2$w to PD; 4) DTI to registered $T_2$W. First, the DW images were registered to the b=0 image to correct for spatial distortions in the DW images. This was done with the Philips Research Imaging Development Environment (PRIDE) Diffusion Registration tool (version 0.4) using an affine transformation. Thereafter all described processing procedures were performed using Matlab version 7.4.0 (The Mathworks, Inc. Natick MA). To correct for offsets between DTI stacks, neighboring slices from adjacent stacks were registered to one another using mutual information based rigid registration

(9,10). The second and fourth stacks were registered to the middle stack and the first and last stacks were registered to the second and fourth stacks, respectively. The $T_2$W images were registered to the PD images, serving as an intermediate for the registration of the DTI stacks to the anatomical PD images. Next, the registered middle three DTI stacks were registered to the registered $T_2$W images using mutual information based rigid registration (9,10). Finally, all transformation matrices were combined to transform the original DTI images, preventing multiple interpolation steps. The diffusion gradient directions were corrected for the combined image transformations. Thereafter, the tensor calculations were performed.

### Fiber tracking

Fiber tracking was essentially performed as described previously (4). The borders of the TA were tracked from the anatomical PDw images. The positions of both the superficial and deep aspects of the central aponeurosis were manually digitized for each slice. For each side, the average position of the digitized aponeurosis was determined by using linear filtering through convolution. 3D mesh reconstructions of both sides of the aponeurosis were defined with 200 rows × 100 column density and the points of intersection were used as seed points for fiber tracking. Fiber tracking was performed by following the direction of greatest diffusion from the seed points along each of the deep and superficial aspects of the TA's aponeurosis. Proper accounting was made for the 4:1 slice: in plane resolution aspect ratio.

The SNR at the aponeurosis is low and partial volume effects artifacts between the superficial and deep compartments can occur. Therefore the eigenvector of each voxel at the aponeurosis and the neighboring voxel were replaced by the eigenvector values of the voxel at one voxel lateral displacement. Fibers were terminated at the muscle borders, if FA<0.15 or FA>0.75, or if successive points had a curvature of >45°. The influence of these settings were investigated by evaluating the fiber tracking with either FA= 0.05, 0.10, 0.15, 0.2, 0.25, or 0.3 and curvature = 45°; and curvature = 10, 20, 30, 40, 50, 60, 70, or 80 degrees and FA = 0.15.

The fiber length was calculated as follows. The x, y, and z positions of the fiber as function of point number were fitted to a third-order polynomial. The sum of the distance between consecutive fitted points represents the fiber length.

### Statistics

Because the mesh is defined by a fixed number of rows and columns but its width varies with position, each fiber tract represents a different amount of aponeurosis area. Therefore, the percentages were adjusted by the actual aponeurosis area represented by the tract.

Linear regression between the calculated percentages and subject characteristics were performed in SPSS 15.0 (Chicago, IL).

## Results

Figure 2A shows the reconstructed fiber tracts prior to the quantitative assessment of fiber tracking. Very short tracts can be observed in the distal portion of the muscle and fiber tracts that erroneously cross over to the opposite side of the aponeurosis can be observed in the middle and proximal portions of the muscle. Table 1 shows that in the superficial compartment of the muscle, $FT_{Short}$= 2 ± 2%, $FT_{Crossed}$= 1 ± 1%, $FT_{Length}$= 5 ± 4%, and $FT_{Premature}$= 3 ± 6%; for the deep compartment, $FT_{Short}$= 2 ± 1%, $FT_{Crossed}$= 15 ± 17%, $FT_{Length}$= 4 ± 3%, and $FT_{Premature}$= 4 ± 7%. In the superficial and deep compartments, 89.4 ± 9.6% and 75.0 ± 15.2% of the tracked aponeurosis area were represented by complete fiber tracts, respectively. Figure 2B shows only the $FT_{Complete}$ fiber tracts.

The distribution of the fiber tracking assessment along the aponeurosis shows that inaccurate fibers tended to be grouped (Figure 3). In all subjects and in both compartments, short fibers occurred primarily at the distal end of the aponeurosis. In the deep portion of the muscle, $FT_{Crossed}$ tracts tended to occur along the whole aponeurosis with an emphasis on the distal to middle areas, whereas for the superficial compartment they were most frequent in the distal area. In both compartments, $FT_{Premature}$ tracts were mainly present at the proximal portion of the aponeurosis and/or along lines. $FT_{Length}$ were throughout the aponeurosis and could be clustered along lines. No significant correlation was present between any of the assessment percentages and the subject length, weight, muscle volume, muscle length or maximal cross-sectional area (highest $r^2$=0.232, p=0.227). However, for the subject with high $FT_{Premature}$ spatial warping was most severe and image registration was poor, both resulting in inaccurate fiber tracking.

We also assessed the fiber tracking for a range of curvature or FA settings (Figure 4). At low curvature settings, fewer fibers were tracked and the percentages of short and premature fibers were high. $FT_{Complete}$ increased with higher curvature settings until it reached an asymptote. A similar pattern is present with increasing FA values resulting in fewer tracked fibers and higher percentages of $FT_{less}$ and $FT_{Premature}$. The number of tracked fibers drastically drops with an FA of 0.3 for the superficial compartment and 0.25 for the deep compartment, although a decrease is already present at a lower FA value.

## Discussion

This paper describes a procedure for quantitative assessment of DTI-based muscle fiber tracking. This assessment was performed on the TA muscle and revealed that the majority of fibers were tracked completely and inaccurate fibers were mostly grouped. The effects of different stop criteria, FA and curvature, were also investigated. The assessment algorithm will enable further studies towards accurately quantifying muscle architectural parameters, assessing the quality of new fiber tracking algorithms, or using DTI-based muscle fiber tracking data in mechanical models of muscle.

Several improvements have been made compared to our previous paper (4), including acquisition, image registration, and mesh definition. The major improvements in the acquisition were the use of ten gradient directions to improve the eigenvector determination and the use of surface coils to obtain higher SNR. SNR levels were assessed using procedures described by Dietrich *et al.* (11) finding mean SNR levels of 106 and 147 for superficial and deep compartments, respectively. These SNR levels were above the estimated SNR of 100 required to obtain an angular uncertainty of the principal eigenvector of ± 5° in single voxels (12). Image registration improved the alignment of consecutive stacks and of the DTI with the anatomical images. The mesh definition was improved in two ways. First, both sides of the aponeurosis were defined separately to account for the increasing aponeurosis thickness at the distal end, thereby enabling fiber tracking directly from the aponeurosis. Secondly, smoothing the mesh accounted for small variations in the manual point selections. Although no quantitative comparison was made between these and our previous data, we expect that all of these improvements resulted in better and more accurate fiber tracking.

The described algorithm contains multiple steps to exclude or include fibers and takes many possible reasons for inaccurate fibers into account. The definition that correct fibers stop within two voxels of the muscle border includes fibers that stop because of curvature or FA relating to the muscle edge. While this might be expected to lead to a higher percentage of complete fibers for muscles with a smaller CSA, there was no correlation between CSA and $FT_{Complete}$ across a 1.9-fold range of CSA. Fibers that crossed into the other compartment

($FT_{Crossed}$) were assessed by forming masks next to the positions of the aponeurosis, resulting in an estimate of the compartments. This approach is fast, but might not be completely inclusive and few inaccurate fibers at the edges might be missed (although in practice, none were observed). The assessment can be extended to other muscles, but depending on their architecture small adjustments may be required. For example, uni-pennate muscles won't show $FT_{crossed}$, while for small muscles the border criteria for $FT_{complete}$ will include most fibers.

The criteria for rejected fibers tended to be spatially clustered, which can be expected if there are similar, spatially dependent underlying architectural or artifactual bases for the deviation from typical tracking results. Short fibers were primarily present at the distal end of the aponeurosis, where the CSA is small and the mask stops fiber tracking after a small number of points. The larger $FT_{Crossed}$ for the deep compartment may be caused by the small pennation angle (~10°) of the deep fibers; therefore, small levels of angular uncertainty in the principal eigenvector would create a possibility of incorrectly tracking fibers from the deep into the superficial compartment. The distribution of both $FT_{Premature}$ and $FT_{Length}$ occurs along lines following the length of the aponeurosis. This can be attributed to the same slice and voxels causing problems in fiber tracking, but different path lengths before this point is reached.

The quantitative assessment data need to be interpreted with caution as multiple factors, including subject characteristics, acquisition settings, imaging artifacts, and fiber tracking algorithm, can contribute to the presence of inaccurate fibers. It may be that a high percentage of $FT_{Premature}$ can be attributed to imaging artifacts, as seen for subject 7, which could be a warning sign for a bad dataset. Exclusion of this dataset did not improve a possible correlation between the percentages and the subject characteristics. In the future non-rigid registration of the DTI stacks or the DTI to the anatomical images might correct some non-linear distortions and improve the fiber tracking. Further research is needed to understand the relation between the assessment criteria and the underlying anatomical or artifactual causes. The same holds for the effect of the fiber tracking algorithm on the resulting quality percentages. It can be expected that with nearest neighbor interpolation or a more sophisticated use of the stop criteria, the $FT_{Premature}$ would be lower as the effect of one incorrect pixel is more diminished. Probabilistic methods might result in lower percentages of $FT_{Crossed}$ as this method investigates the probability of fiber trajectories based on the angular uncertainty for each voxel; therefore, addition trajectories might be found along the aponeurosis that remain within the compartment, which otherwise might cross over to the other compartment using the described deterministic approach.

The assessment provides a mean to evaluate the effects of different stop criteria settings (FA and curvature) on the resulting fibers. As expected, fiber tracking is poor with low curvature or high FA settings and the change in the percentages is minimal at curvature settings $\geq 45°$ or $FA \leq 0.15$, suggesting that these would make suitable stop criteria. However, for different muscles or for diseased muscle these values might differ as either the underlying fiber curvature can be higher or lower than for the TA (13–15) or the diffusivities or FA values can be altered (16–19).

In summary, we have presented a method for quantitative assessing DTI muscle fiber tractography results. The method is based on expected patterns of muscle fiber geometry, including similar local fiber orientations and the tendency of muscle fascicles to extend completely from origin to insertion, and changes in diffusion characteristics or image artifacts that might lead to premature fiber tract termination. Applications of the method include the exclusion of erroneous fiber tracking results, the quantitative assessment of data set quality, and the assessment of fiber tracking stop criteria. Further additional application

of this method may include the determination of suitable stop criteria in studies of diseased or injured muscle and the assessment of muscle fiber tracking methods.

## Acknowledgments

**Grant support**

NIH/NINDS R01 NS034834; NIH/NIAMS AR050101; NIH/NCRR M01 RR 00095

## References

1. Damon BM, Ding Z, Anderson AW, Freyer AS, Gore JC. Validation of diffusion tensor MRI-based muscle fiber tracking. Magn Reson Med. 2002; 48(1):97–104. [PubMed: 12111936]
2. Heemskerk AM, Strijkers GJ, Vilanova A, Drost MR, Nicolay K. Determination of mouse skeletal muscle architecture using three-dimensional diffusion tensor imaging. Magn Reson Med. 2005; 53(6):1333–1340. [PubMed: 15906281]
3. Sinha S, Sinha U, Edgerton VR. In vivo diffusion tensor imaging of the human calf muscle. J Magn Reson Imaging. 2006; 24(1):182–190. [PubMed: 16729262]
4. Lansdown DA, Ding Z, Wadington M, Hornberger JL, Damon BM. Quantitative diffusion tensor MRI-based fiber tracking of human skeletal muscle. J Appl Physiol. 2007; 103(2):673–681. [PubMed: 17446411]
5. Heemskerk AM, Damon BM. Diffusion tensor MRI assessment of skeletal muscle architecture. Current Medical Imaging Reviews. 2007; 3(3):152–160.
6. Hori M, Ishigame K, Shiraga N, Kumagai H, Aoki S, Araki T. Mean diffusivity, fractional anisotropy maps, and three-dimensional white-matter tractography by diffusion tensor imaging. Comparison between single-shot fast spin-echo and single-shot echo-planar sequences at 1.5 Tesla. Eur Radiol. 2008; 18(4):830–834. [PubMed: 17999065]
7. Mori S, van Zijl PC. Fiber tracking: principles and strategies - a technical review. NMR in biomedicine. 2002; 15(7–8):468–480. [PubMed: 12489096]
8. Jones DK, Horsfield MA, Simmons A. Optimal strategies for measuring diffusion in anisotropic systems by magnetic resonance imaging. Magn Reson Med. 1999; 42(3):515–525. [PubMed: 10467296]
9. Viola P, Wells WM 3rd. Alignment by Maximization of Mutual Information. International Journal of Computer Vision. 1997; 24(2):17.
10. Studholme C, Hill DLG, Hawkes DJ. An overlap invariant entropy measure of 3D medical image alignment. Pattern Recognition. 1999; 32(1):15.
11. Dietrich O, Raya JG, Reeder SB, Reiser MF, Schoenberg SO. Measurement of signal-to-noise ratios in MR images: influence of multichannel coils, parallel imaging, and reconstruction filters. J Magn Reson Imaging. 2007; 26(2):375–385. [PubMed: 17622966]
12. Damon BM. Effects of Image Noise in Muscle DT-MRI Assessed Using Numerical Simulations. MRM. 2008 in press.
13. Manal K, Roberts DP, Buchanan TS. Optimal pennation angle of the primary ankle plantar and dorsiflexors: variations with sex, contraction intensity, and limb. Journal of applied biomechanics. 2006; 22(4):255–263. [PubMed: 17293622]
14. Lieber RL, Friden J. Functional and clinical significance of skeletal muscle architecture. Muscle & nerve. 2000; 23(11):1647–1666. [PubMed: 11054744]
15. Lieber RL, Friden J. Clinical significance of skeletal muscle architecture. Clinical orthopaedics and related research. 2001; (383):140–151. [PubMed: 11210948]
16. Heemskerk AM, Strijkers GJ, Drost MR, van Bochove GS, Nicolay K. Skeletal muscle degeneration and regeneration after femoral artery ligation in mice: monitoring with diffusion MR imaging. Radiology. 2007; 243(2):413–421. [PubMed: 17384238]
17. Saotome T, Sekino M, Eto F, Ueno S. Evaluation of diffusional anisotropy and microscopic structure in skeletal muscles using magnetic resonance. Magnetic resonance imaging. 2006; 24(1): 19–25. [PubMed: 16410174]

18. Zaraiskaya T, Kumbhare D, Noseworthy MD. Diffusion tensor imaging in evaluation of human skeletal muscle injury. J Magn Reson Imaging. 2006; 24(2):402–408. [PubMed: 16823776]
19. Qi J, Olsen NJ, Price RR, Winston JA, Park JH. Diffusion-weighted imaging of inflammatory myopathies: Polymyositis and dermatomyositis. J Magn Reson Imaging. 2008; 27(1):212–217. [PubMed: 18022843]

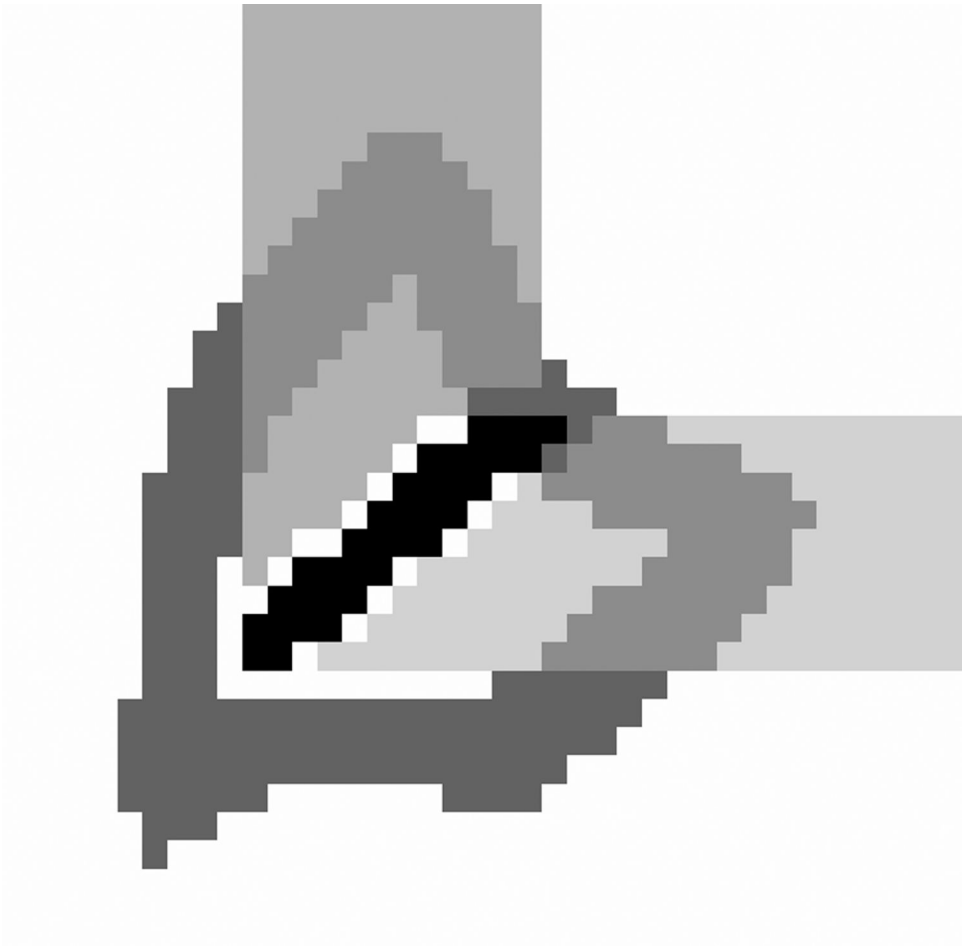

**Figure 1.**
Example of the masks to determine the quantitative assessment. The aponeurosis is indicated in black and the derived masks for the superficial (medium grey) and deep (light grey) compartments. The near border mask is indicated in dark grey.

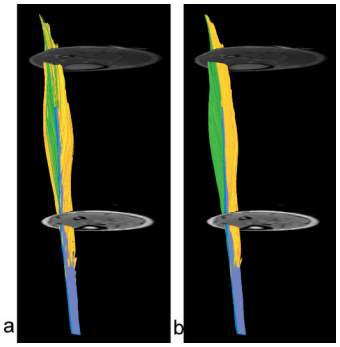


**Figure 2.**
Fiber trajectories for subject 3 before (a) and after (b) quantitative assessment. Note the yellow fibers in both compartments in a. The aponeurosis is indicated in blue and fibers originating from the deep aspect of the aponeurosis are indicated in shades of yellow, while fibers originating from the superficial aspect of the aponeurosis are indicated in shades of green. Color variations within the tracts exist only for contrast.

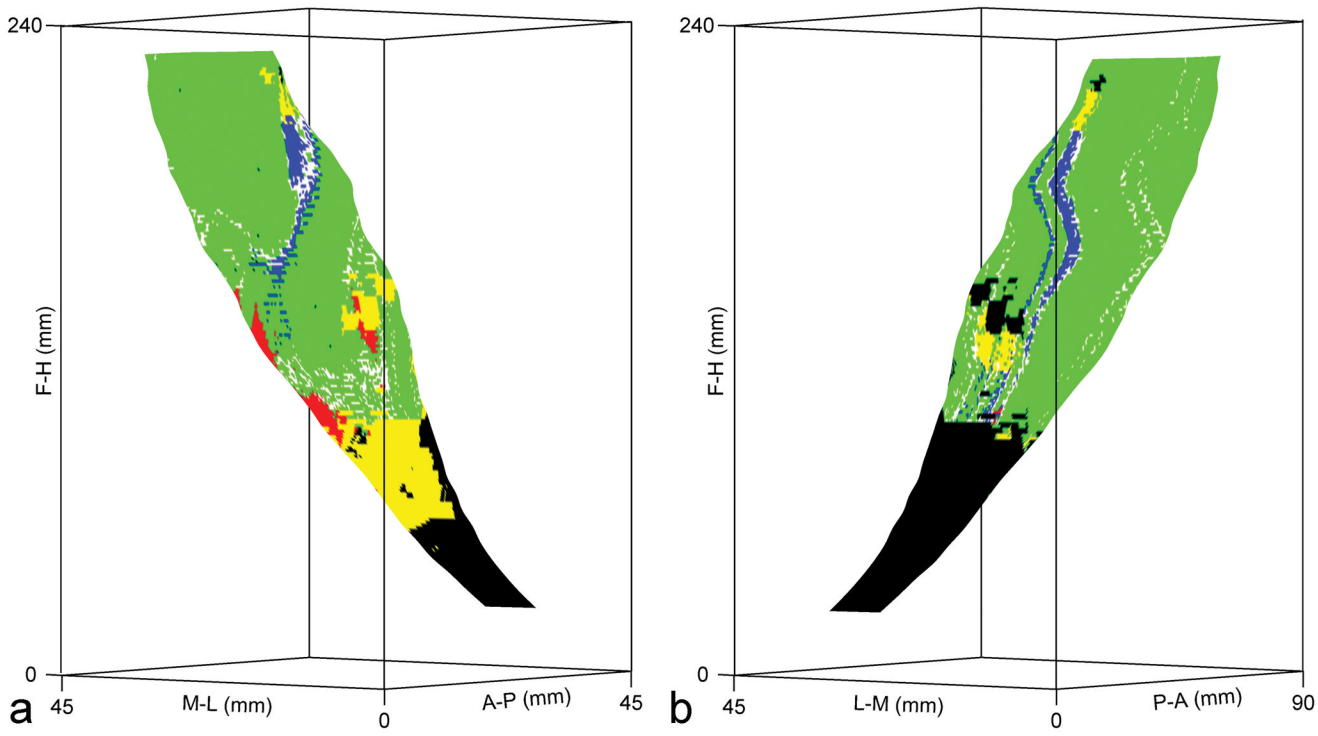


**Figure 3.**

Three dimensional representation of the aponeurosis, with colors indicating fiber tract assessment. The distributions are depicted for the deep (a) and superficial (b) aspects of the aponeurosis for subject 3. The perspective is 180° rotated between the two. $FT_{Complete}$: green; $FT_{less}$: yellow; $FT_{Crossed}$: red; $FT_{Length}$: white; $FT_{Premature}$: blue; not tracked: black.

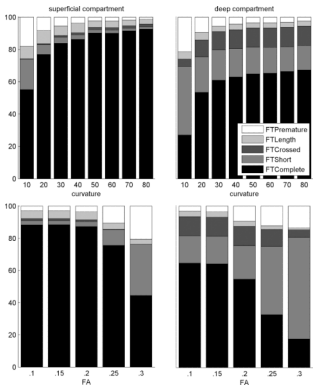


**Figure 4.**
Quantitative assessment percentages. Percentages are displayed as function of curvature (upper) or FA (bottom) and for the superficial (right) and deep (left) compartment.

**Table 1**

Aponeurosis area percentages of complete and inaccurate fibers for both compartments

| | Superficial aponeurosis | | | | | Deep aponeurosis | | | | |
|---|---|---|---|---|---|---|---|---|---|---|
| **subjects** | **$FT_{Complete}$** | **$FT_{Short}$** | **$FT_{Crossed}$** | **$FT_{Length}$** | **$FT_{Premature}$** | **$FT_{Complete}$** | **$FT_{Short}$** | **$FT_{Crossed}$** | **$FT_{Length}$** | **$FT_{Premature}$** |
| 1 | 79.9 | 0.0 | 4.4 | 12.4 | 3.3 | 83.7 | 0.6 | 0.0 | 5.9 | 9.7 |
| 2 | 97.5 | 0.0 | 0.5 | 1.9 | 0.0 | 53.4 | 0.8 | 45.3 | 0.4 | 0.0 |
| 3 | 85.1 | 3.3 | 0.1 | 6.3 | 5.2 | 80.0 | 2.9 | 6.0 | 7.8 | 3.4 |
| 4 | 95.0 | 1.9 | 0.0 | 3.1 | 0.0 | 67.2 | 1.8 | 29.7 | 1.4 | 0.0 |
| 5 | 95.3 | 0.0 | 0.1 | 4.6 | 0.0 | 93.3 | 1.0 | 0.0 | 5.6 | 0.2 |
| 6 | 95.0 | 2.4 | 0.0 | 1.3 | 1.3 | 85.7 | 0.6 | 3.8 | 4.7 | 5.2 |
| 7 | 69.1 | 5.9 | 0.2 | 7.8 | 17.0 | 54.2 | 4.9 | 17.3 | 3.7 | 19.9 |
| 8 | 91.3 | 2.7 | 1.8 | 4.3 | 0.0 | 91.5 | 1.1 | 0.0 | 6.8 | 0.6 |
| 9 | 96.8 | 0.9 | 0.6 | 1.7 | 0.0 | 66.0 | 1.2 | 30.7 | 2.1 | 0.0 |
| Mean | 89.4 | 1.9 | 0.8 | 4.8 | 3.0 | 75.0 | 1.7 | 14.7 | 4.3 | 4.3 |
| SD | 9.6 | 1.9 | 1.4 | 3.6 | 5.6 | 15.2 | 1.4 | 16.8 | 2.5 | 6.7 |

*Magn Reson Med*. Author manuscript; available in PMC 2010 February 1.